In Protocol 4, the performance of the feedback controller was evaluated by the time required for the AP response to reach 90% of the target AP decrease and by the standard deviation of the steady-state error between the target and measured AP values during the last 5 min of the 10-min feedback control. These two values were calculated based on the 2-s moving averaged data of AP.

Statistical analysis

All data are presented as means and SE values. In Protocol 1, changes in AP were examined by two-way repeated-measures analysis of variance (ANOVA) using the stimulus current as one factor and the pulse width as the other factor.[22] In Protocol 2, changes in AP were examined by two-way repeated-measures ANOVA using the stimulus frequency as one factor and the pulse width as the other factor. Differences were considered significant when P<0.05.

Results

Relationship Between Stimulus Intensity and AP Response

Typical time series of Protocols 1 and 2 obtained from one animal are shown in Figures 2A and 2B, respectively. The pulse width was set in a random order. In Protocol 1, baseline AP obtained at the 0-mA stimulus condition was 118.4±5.4 mmHg across the animals. Changes in mean AP as a function of stimulus current are summarized in Figure 2C. The decrease in AP became greater as the stimulus current increased. The overall statistical analysis indicated that the effect of the stimulus current on the magnitude of AP decrease was significant whereas that of pulse width was not. There was no significant interaction effect between the stimulus current and the pulse width.

In Protocol 2, baseline AP at the 0-Hz stimulus condition was 117.6±5.9 mmHg across the animals. Changes in mean AP as a function of stimulus frequency are summarized in Figure 2D. The decrease in AP became greater as the stimulus frequency increased from 1 to 10 Hz but it became smaller when the stimulus frequency exceeded 10 Hz. At the pulse width of 1 ms, the stimulus frequency of 100 Hz even increased AP. The overall statistical analysis indicated that the effect of stimulus frequency on the magnitude of AP decrease was significant whereas that of pulse width was not. There was no significant interaction effect between the stimulus frequency and the pulse width.

Dynamic Characteristics of AP Response to HES

Figure 3A depicts typical time series obtained from Protocol 3. HES was turned on and off randomly, which decreased the mean level of AP and also caused intermittent AP variations. When HES was finally turned off at 30 min, AP began to increase toward the prestimulation value. A long-lasting effect of HES was not observed in the present protocol. The white line in the AP trace represents the 2-s moving averaged data of AP.

The results of transfer function analysis are depicted in Figure 3B. In the gain plot, the magnitude of AP response relative to the HES input was plotted in the frequency domain. The gain value became smaller as the frequency increased, indicating the low-pass characteristics of the AP response to HES. In the phase plot, AP showed an out-of-phase relationship with HES at the lowest frequency (0.0024 Hz). The phase delayed more with increasing the frequency of modulation. The coherence value was approximately 0.7 in the frequency range below 0.06 Hz. The coherence value became smaller in the frequency range above 0.1 Hz but still retained a value of 0.5, indicating that approximately half of the AP variation was explained by the HES input.

The general feature of the dynamic characteristics of the AP response to HES approximated what is known as a second order low-pass filter with a pure dead time, which is mathematically described as

$$H(f) = \frac{-K}{1 + 2\zeta\dfrac{f}{f_N}j + \left(\dfrac{f}{f_N}j\right)^2} \exp(-2\pi f j L) \tag{3}$$

where K is the steady-state gain, f_N is the natural frequency, ζ is the damping ratio, and L is the pure dead time. When we performed an iterative nonlinear least square fitting using a downhill Simplex method, K, f_N, ζ and L were estimated as 10.2 ± 1.6 mmHg/mA, 0.040 ± 0.004 Hz, 1.80 ± 0.24 and 1.38 ± 0.13 s, respectively. A model transfer function shown in Figure 3C was drawn using K, f_N, ζ and L of 10 mmHg/mA, 0.04 Hz, 2 and 1 s, respectively.

Development of Feedback Controller

We used a classical feedback controller to adjust the stimulus intensity of HES.[23-25] In reference to Figure 4A, a HES command is determined based on a difference between measured and target AP values. $G(f)$ represents the transfer function of the controller with a proportional gain (K_P) and an integral gain (K_I). $H(f)$ indicates the model transfer function shown in Figure 3C. A detailed mathematical description of the controller is supplied in *Appendix A*.

To circumvent a threshold phenomenon in the stimulus current-AP response relationship (see *Appendix B* for details), the HES command (in an arbitrary unit) was transformed into the stimulus current (in mA) by a factor of 1 (Fig. 4B, left) only when the HES command exceeded unity. When the HES command was less than unity, the stimulus current was held at 1 mA and the HES command was transformed into the stimulus frequency (in Hz) by a factor of 10 (Fig. 4B, right). The stimulation was turned off when the HES command became negative.

Several sets of simulations were conducted using the model transfer function. The target AP was set at 20 mmHg below the baseline AP. To mimic the pulse pressure in AP, a 3-Hz sinusoidal wave (corresponding to the HR of 180 beats/min) with an amplitude of 15 mmHg (corresponding to the pulse pressure of 30 mmHg) was added to the AP signal. To avoid pulsatile variation in the HES command, we set the proportional gain at zero. Under this condition, when the integral gain was set at 0.001, AP decreased gradually and it took more than 3 min to reach the target AP (Fig. 4C, left). When the integral gain was set at 0.005, AP decreased more promptly and reached the target AP in less than one minute (Fig. 4C, center). When the integral gain was set at 0.01, the AP response occurred more rapidly but showed significant oscillations before settling (Fig. 4C, right). Based on these simulation results, we set the proportional gain at zero and the integral gain at 0.005 for the actual feedback-control experiment in Protocol 4.

Performance of feedback controller

Figure 5A demonstrates the AP regulation by HES obtained from 2 typical animals. The proportional and integral gains of the controller were not altered among the animals (i.e., $K_P = 0$, $K_I = 0.005$). The white line in the AP trace indicates 2-s moving averaged data. The target AP was set at 20 mmHg below the AP value just before the application of HES. The feedback controller was activated for 10 min, which decreased AP at the target level. The HES command was individualized via the feedback mechanism. In the left panel of Figure 5A, the HES command gradually increased throughout the 10-min regulation. In the right panel of Figure 5A, the HES command was less than unity from 1 to 7 min of the 10-min regulation. In this time period, the HES command altered the stimulus frequency rather than the stimulus current.

Mean and mean±SE values of the HES command averaged from 8 animals are shown in the top panel of Figure 5B. There was a large variance in the HES command among the animals, suggesting inter-individual differences in the responsiveness to HES. The target AP was 102.5 ± 5.6 mmHg across the animals. The error signal between the target AP and measured AP disappeared in less than one minute (Figure 5B, bottom). The time required for the AP response to reach 90% of the target AP decrease was 38 ± 10 s. Thereafter, the error remained very small

until the end of the 10-min regulation. The standard deviation of the steady-state error was 1.3±0.1 mmHg. After the end of the feedback regulation, the error signal gradually returned to approximately 20 mmHg.

Figure 6 represents typical results of the supplemental protocols. Electrical stimulation of the triceps surae muscle (denoted as "MS") did not change AP significantly in spite of visible twitching of the stimulated muscle, suggesting that the depressor response to HES was not the outcome of the direct muscle stimulation (Fig. 6A). Sectioning the ipsilateral sciatic nerve abolished the depressor effect of HES, suggesting that somatic afferent signals were delivered through the sciatic nerve to the central nervous system during HES (Fig. 6B).

Discussion

We identified the dynamic input-output relationship between HES and the AP response. By using the model transfer function from HES to AP, we were able to develop a servo-controller that automatically adjusted the HES command to reduce AP at a prescribed target level.

Development of Feedback Controller

The stimulus current-AP response relationship showed a monotonous decreasing slope (Fig. 2C). Because the effect of the pulse width was statistically insignificant, we chose the stimulus current as a primary control variable. The problem with using the stimulus current for the control variable was that a certain threshold current existed between 0 and 1 mA where the AP response to EA became discontinuous. If the stimulus current happened to be feedback controlled near the threshold current, AP showed significant oscillation around the target level (Fig. 7, see *Appendix B* for details). To avoid such a problem related to the threshold current, we set the minimum current to 1 mA (above the threshold current) and employed the stimulus frequency as a secondary control variable (Fig. 4B).

The stimulus frequency-AP response relationship revealed a valley-shaped curve with the nadir around 10 Hz (Fig. 2D). The result is similar to that obtained by stimulating hamstring muscle afferent nerves.[26] From the viewpoint of controller design, the valley-shaped input-output relationship is troublesome because the proportional-integral controller only assumes a monotonous input-output relationship.[23] To avoid the problem of the valley-shaped input-output relationship, we limited the stimulus frequency to the range from 0 to 10 Hz (Fig. 4B, right). A similar strategy of selecting the monotonous input-output portion was employed in a previous study.[12]

We quantified the dynamic AP response to HES using a transfer function analysis (Fig. 3B), and modeled it by a second-order low-pass filter with a pure dead time (Fig. 3C). Once the transfer function is modeled, we can construct a numerical simulator for the feedback controller design (Fig. 4A). Because the optimization of control parameters usually requires a number of trials even if the initial values are selected via classical methods such as Ziegler-Nichols' method,[23] it is impractical to determine optimal parameter values without using the simulator. The simulation results indicated that the integral gain value of 0.005 would provide rapid and stable AP regulation (Fig. 4C). Because the controller was designed via intensive simulations, AP was actually controlled at the target level with a small variance (Fig. 5B, bottom panel). Note that the current and frequency of HES were automatically adjusted and individualized via the feedback mechanism (Fig. 5A).

Bionic Strategies Using Neural Interfaces

A framework of treating cardiovascular diseases using neural interfaces is intriguing because the autonomic nervous system exerts powerful influences on the circulatory system. In previous studies, we identified the dynamic characteristics of the arterial baroreflex system and used them to design an artificial vasomotor center. The artificial vasomotor center was able to

control AP by stimulating the celiac ganglia in anesthetized rats[10,11] or the spinal cord in anesthetized cats.[12] The strength and rapidity of the neural effect on the cardiovascular system compared with that of the humoral effect[27,28] make the neural interventions desirable for the rapid and stable restoration of AP against acute disturbances such as those induced by postural changes. Gotoh et al. demonstrated that a direct neural interface to the rostral ventrolateral medulla also enabled rapid and stable restoration of AP during nitroprusside-induced hypotension in conscious rats.[29] The bionic system to control AP has also been applied in human subjects.[13]

Although the aforementioned bionic systems aimed to maintain AP against acute hypotension by increasing sympathetic nerve activity,[10-13,29] sympathoinhibition may also be required for the treatment of cardiovascular diseases accompanying sympathetic overactivity. Baroreceptor activation is one of the potential sympathoinhibitory neural modulation.[8,9] In the present study we only demonstrated a framework of short-term AP control by HES. With a development of proper implanting electrodes, however, we may be able to control AP chronically using HES. Although carotid sinus baroreceptor stimulation has a potential to treat drug-resistant hypertension,[9] it could activate peripheral chemoreflex by stimulating carotid bodies. HES may circumvent such unintentional chemoreflex activation. Another clinical implication will be the treatment of chronic heart failure. Although the vagal effect of HES was not evaluated in the present study, acupuncture stimulation may facilitate cardiac vagal activity.[30] Because chronic intermittent vagal nerve stimulation increased the survival of chronic heart failure rats,[7] chronic intermittent HES may be used as an alternative method of direct vagal nerve stimulation for the treatment of chronic heart failure.

Limitations

First, we did not identify the mechanism of HES. Because sectioning of the ipsilateral sciatic nerve abolished the AP response to HES (Fig. 6B), somatic afferent is involved in the effect of HES. In a series of studies, Longhurst et al. demonstrated that electroacupuncture activated group III and IV fibers in the median nerves and inhibited sympathetic outflow via activation of μ- and δ-opioid receptors in the rostral ventrolateral medulla.[31,32] Whether the similar mechanism underlies in the rapid-onset and short-lasting effect of HES awaits further studies.

Second, we used pentobarbital anesthesia. Although peripheral neurotransmissions of norepinephrine and acetylcholine can be assessed under the same anesthesia,[28,33] because pentobarbital can suppress many neurotransmitters in the central nervous system,[34] anesthesia may compromise the HES effect. Further studies are required to establish the utility of HES in awake conditions.

Third, we set the proportional gain of the controller at zero to avoid pulsatile changes in the HES command. However, other approaches such as that using a low-passed signal of measured AP as a controlled variable might also be effective to avoid the pulsatile variation in the HES command.

Finally, a development of implanting electrodes is the prerequisite for chronic use of HES. Intramuscular electrodes used in functional electrical stimulation might be used for HES but further refinements are clearly needed regarding the positioning of electrodes including the depth of implantation.[35, 36]

In conclusion, we identified the dynamic characteristics of the AP response to acupuncture-like HES and demonstrated that a servo-controlled HES system was able to reduce AP at a prescribed target level. Although further studies are required to identify the mechanism of HES to reduce AP, acupuncture-like HES would be an additional modality to exert quantitative depressor effect on the cardiovascular system.

Appendix A
Framework of Feedback Controller

Figure 4A is a simplified block diagram of the feedback controller system utilized in the present study. The controller was based on a proportional-integral controller.[23-25] $G(f)$ represents the transfer function of the controller.

$$G(f) = -K_P + \frac{-K_I}{2\pi f j} \tag{A1}$$

where K_P and K_I denote proportional and integral gains, respectively. j represents the imaginary unit. Negative signs for the proportional and integral gains compensate for the negative input-output relationship between HES and the AP response. $H(f)$ represents a model transfer function from HES to AP determined from Protocol 3. The measured AP can be expressed as

$$AP_{Measured}(f) = H(f)HES(f) + AP_{Noise}(f) \tag{A2}$$

where $AP_{Noise}(f)$ is the AP fluctuation such as that associated with changes in animal conditions. The controller compares the measured AP with the target AP, and adjusts the HES command to minimize the difference between them according to the following equation.

$$HES(f) = G(f)[AP_{Target}(f) - AP_{Measured}(f)] \tag{A3}$$

By eliminating $HES(f)$ from the equations A2 and A3, the overall controller characteristics are described as

$$AP_{Measured}(f) = \frac{G(f)H(f)}{1 + G(f)H(f)} AP_{Target}(f) + \frac{1}{1 + G(f)H(f)} AP_{Noise}(f) \tag{A4}$$

The equation A4 indicates that if $G(f)$ is properly selected so that $G(f)H(f)$ becomes by far greater than unity, the measured AP approaches the target AP whereas the noise term is significantly attenuated over the frequency range of interest.

Appendix B
Problem with Threshold Current

We tried to adjust the intensity of HES by the stimulus current alone. When the stimulus current happened to be feedback controlled near a threshold current, however, the controller showed on-off type controller behavior around the target AP level as shown in Figure 7. At time zero, the controller was activated. The stimulus current increased to approximately 2.7 mA in the beginning and then decreased to a value below 1 mA, accompanying the AP reduction around a target level (a horizontal dashed line). However, the stimulus current and AP did not stabilize. Because the AP response was discontinuous at the threshold current (i.e., the depressor effect of HES was abruptly turned on and off), the controller could not adjust the stimulus current in a continuous manner. To avoid this kind of on-off type controller behavior, we introduced the stimulus frequency as the secondary control variable (Fig. 4B).

References
1. Bilgutay AM, Bilgutay IM, Merkel FK, Lillehei CW. Vagal tuning. A new concept in the treatment of supraventricular arrhythmias, angina pectoris, and heart failure. J Thorac Cardiovasc Surg 1968; 56: 71-82.
2. Braunwald E, Epstein SE, Glick G, Wechsler AS, Braunwald NS. Relief of angina pectoris by electrical stimulation of the carotid-sinus nerves. N Engl J Med 1967; 277: 1278-1283.
3. Schwartz SI, Griffith LS, Neistadt A, Hagfors N. Chronic carotid sinus nerve stimulation in the treatment of essential hypertension. Am J Surg 1967; 114: 5-15.
4. Vanoli E, De Ferrari GM, Stramba-Badiale M, Hull SS Jr, Foreman RD, Schwartz PJ. Vagal stimulation and prevention of sudden death in conscious dogs with a healed myocardial infarction. Circ Res 1991; 68: 1471-1481.
5. Yang JL, Chen GY, Kuo CD. Comparison of effect of 5 recumbent positions on autonomic nervous modulation in patients with coronary artery disease. Circ J 2008; 72: 902-908.
6. Baba R, Koketsu M, Nagashima M, Inasaka H, Yoshinaga M, Yokota M. Adolescent obesity adversely affects blood pressure and resting heart rate. CIr J 2007; 71: 722-726.
7. Li M, Zheng C, Sato T, Kawada T, Sugimachi M, Sunagawa K. Vagal nerve stimulation markedly improves long-term survival after chronic heart failure in rats. Circulation 2004; 109: 120-124.
8. Zucker IH, Hackley JF, Cornish KG, Hiser BA, Anderson NR, Kieval R, et al. Chronic baroreceptor activation enhances survival in dogs with pacing-induced heart failure. Hypertension 2007; 50: 904-910.
9. Mohaupt MG, Schmidli J, Luft FC. Management of uncontrollable hypertension with a carotid sinus stimulation device. Hypertension 2007; 50: 825-828.
10. Sato T, Kawada T, Shishido T, Sugimachi M, Alexander J Jr, Sunagawa K. Novel therapeutic strategy against central baroreflex failure: a bionic baroreflex system. Circulation 1999; 100: 299-304.
11. Sato T, Kawada T, Sugimachi M, Sunagawa K. Bionic technology revitalizes native baroreflex function in rats with baroreflex failure. Circulation 2002; 106: 730-734.
12. Yanagiya Y, Sato T, Kawada T, Inagaki M, Tatewaki T, Zheng C, et al. Bionic epidural stimulation restores arterial pressure regulation during orthostasis. J Appl Physiol 2004; 97: 984-990.
13. Yamasaki F, Ushida T, Yokoyama T, Ando M, Yamashita K, Sato T. Artificial baroreflex: clinical application of a bionic baroreflex system. Circulation 2006; 113: 634-639.
14. Li P, Pitsillides KF, Rendig SV, Pan HL, Longhurst JC. Reversal of reflex-induced myocardial ischemia by median nerve stimulation: a feline model of electroacupuncture. Circulation 1998; 97: 1186-1194.
15. Longhurst JC. Electroacupuncture treatment of arrhythmias in myocardial ischemia. Am J Physiol Heart Circ Physiol 2007; 292: H2032-H2034.
16. Lujan HL, Kramer VJ, DiCarlo SE. Electroacupuncture decreases the susceptibility to ventricular tachycardia in conscious rats by reducing cardiac metabolic demand. Am J Physiol Heart Circ Physiol 2007; 292: H2550-H2555.
17. Ohsawa H, Okada K, Nishijo K, Sato Y. Neural mechanism of depressor responses of arterial pressure elicited by acupuncture-like stimulation to a hindlimb in anesthetized rats. J Auton Nerv Syst 1995; 51: 27-35.
18. Uchida S, Shimura M, Ohsawa H, Suzuki A. Neural mechanism of bradycardiac responses elicited by acupuncture-like stimulation to a hind limb in anesthetized rats. J Physiol Sci 2007; 57: 377-382.

19. Michikami D, Kamiya A, Kawada T, Inagaki M, Shishido T, Yamamoto K, et al. Short-term electroacupuncture at Zusanli resets the arterial baroreflex neural arc toward lower sympathetic nerve activity. Am J Physiol Heart Circ Physiol 2006; 291: H318-H326.

20. Yamamoto H, Kawada T, Kamiya A, Kita T, Sugimachi M. Electroacupuncture changes the relationship between cardiac and renal sympathetic nerve activities in anesthetized cats. Auton Neurosci: Basic and Clinical 2008; 144: 43-49.

21. Marmarelis PZ, Marmarelis VZ. Analysis of Physiological Systems. The white noise method in system identification. New York: Plenum, 1978.

22. Snedecor GW, Cochran WG. Statistical Methods (8th ed.). University Press, Ames, Iowa, 1989.

23. Åström K, Hägglund T. PID Controllers: Theory, Design, and Tuning. (2nd ed.). Instrument Society of America, 1995.

24. Kawada T, Sunagawa G, Takaki H, Shishido T, Miyano H, Miyashita H, et al. Development of a servo-controller of heart rate using a treadmill. Jpn Circ J 1999; 63: 945-950.

25. Kawada T, Ikeda Y, Takaki H, Sugimachi M, Kawaguchi O, Shishido T, et al. Development of a servo-controller of heart rate using a cycle ergometer. Heart Vessels 1999; 14: 177-184.

26. Johansson B. Circulatory responses to stimulation of somatic afferents with special reference to depressor effects from muscle nerves. Acta Physiol Scand 1962; Suppl 198: 1-91.

27. Kawada T, Miyamoto T, Miyoshi Y, Yamaguchi S, Tanabe Y, Kamiya A, et al. Sympathetic neural regulation of heart rate is robust against high plasma catecholamines. J Physiol Sci 2006; 56: 235-245.

28. Kawada T, Yamazaki T, Akiyama T, Shishido T, Miyano H, Sato T, et al. Interstitial norepinephrine level by cardiac microdialysis correlates with ventricular contractility. Am J Physiol Heart Circ Physiol 1997; 273: H1107-H1112.

29. Gotoh TM, Tanaka K, Morita H. Controlling arterial blood pressure using a computer-brain interface. Neuroreport 2005; 16: 343-347.

30. Nishijo K, Mori H, Yosikawa K, Yazawa K. Decreased heart rate by acupuncture stimulation in humans via facilitation of cardiac vagal activity and suppression of cardiac sympathetic nerve. Neurosci Lett 1997; 227: 165-168.

31. Chao DM, Shen LL, Tjen-A-Looi S, Pitsillides KF, Li P, Longhurst JC. Naloxone reverses inhibitory effect of electroacupuncture on sympathetic cardiovascular reflex responses. Am J Physiol Heart Circ Physiol 1999; 276: H2127-H2134.

32. Li P, Tjen-A-Looi SC, Longhurst JC. Rostral ventrolateral medullary opioid receptor subtypes in the inhibitory effect of electroacupuncture on reflex autonomic response in cats. Auton Neurosci: Basic and Clinical 2001; 89, 38-47.

33. Kawada T, Yamazaki T, Akiyama T, Li M, Ariumi H, Mori H, et al. Vagal stimulation suppresses ischemia-induced myocardial interstitial norepinephrine release. Life Sci 2006; 78: 882-887.

34. Adachi YU, Yamada S, Satomoto M, Watanabe K, Higuchi H, Kazama T. et al. Pentobarbital inhibits L-DOPA-induced dopamine increases in the rat striatum: An in vivo microdialysis study. Brain Res Bull 2006; 69: 593-596.

35. Guevremont L, Norton JA, Mushahwar VK. Physiologically based controller for generating overground locomotion using functional electrical stimulation. J Neurophysiol 2007; 97: 2499-2510.

36. Hardin E, Kobetic R, Murray L, Corado-Ahmed M, Pinault G, Sakai J, Bailey SN, Ho C, Triolo RJ. Walking after incomplete spinal cord injury using an implanted FES system: A case report. J Rehabil Res Dev 2007; 44: 333-346.
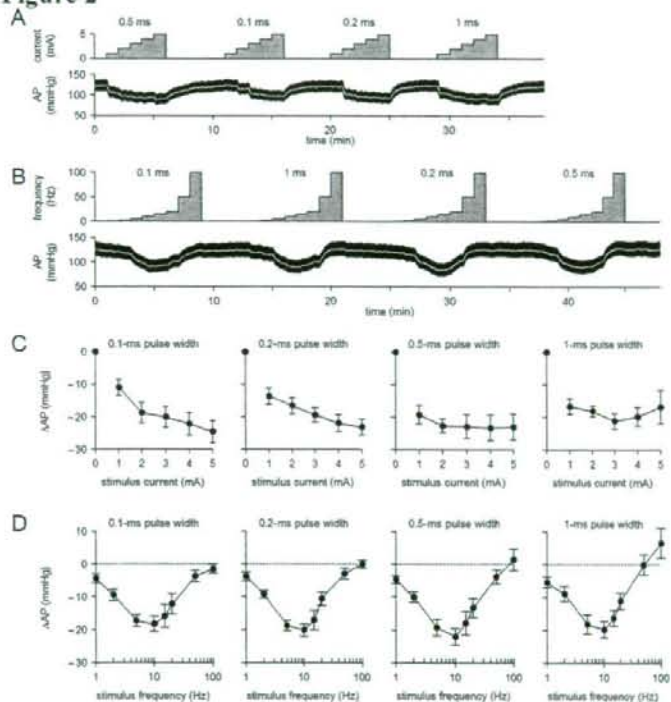
Figure 1
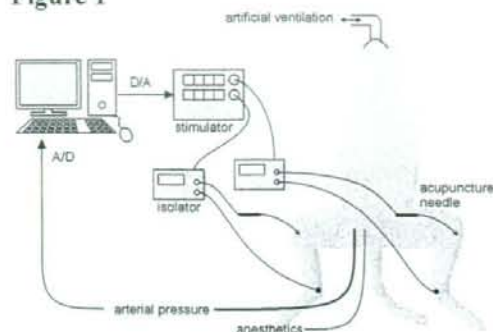
Experimental setup.

Figure 2

A: Typical recordings of Protocol 1 showing the effects of stimulus current and pulse width on arterial pressure (AP). B: Typical recordings of Protocol 2 showing the effects of stimulus frequency and pulse width on AP. The white lines in the AP traces indicate 2-s moving averaged data. C: Changes in AP as a function of the stimulus current. AP decreased monotonously as the stimulus current increased ($P<0.05$). D: Changes in AP as a function of the stimulus frequency. AP decreased more as the stimulus frequency increased from 1 to 10 Hz but the depressor effect became smaller when the stimulus frequency exceeded 10 Hz ($P<0.05$).

Figure 3
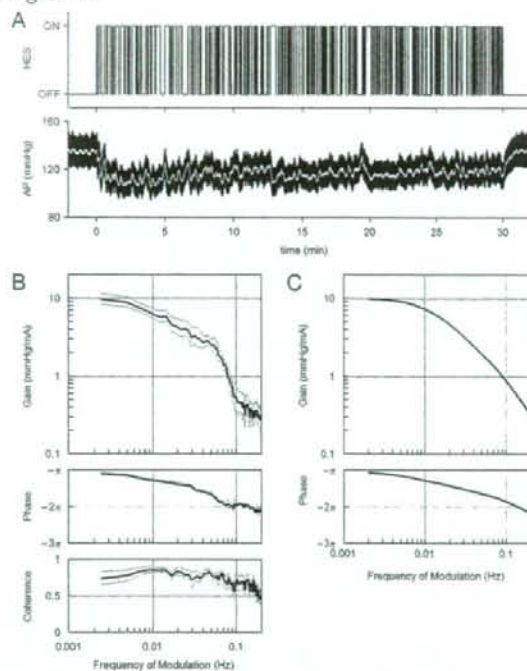
A: Typical recordings of random hind-limb electrical stimulation (HES) and arterial pressure (AP) response. **B:** Transfer function from HES to the AP response averaged from 8 cats. Thick and thin lines indicate mean and mean±SE values, respectively. **C:** A model transfer function of the second-order low-pass filter with a lag time that mimics the transfer function from HES to AP.

Figure 4
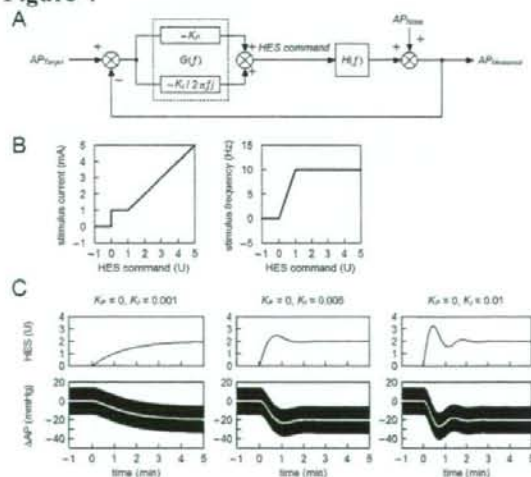
A: A simplified diagram of the feedback controller utilized in the present study. AP_{Target}: target arterial pressure (AP). AP_{Noise}: noise in AP in terms of the control theory. $AP_{Measured}$: measured AP. $G(f)$: transfer function of the controller. $H(f)$: transfer function from hind-limb electrical stimulation (HES) to the AP response. K_P: proportional gain. K_I: integral gain. f and j denote the frequency and imaginary unit, respectively (see *Appendix A* for details). **B:** Functions that convert the HES command into the stimulus current and the stimulus frequency. **C:** Simulation results showing the feedback control of AP by HES. At time zero, the target AP was set at −20 mmHg. In the simulation, a sinusoidal wave (3 Hz, 15 mmHg in amplitude) was added to mimic the pulse pressure in AP. White lines indicate the 2-s moving averaged data of the simulated AP response.

Figure 5
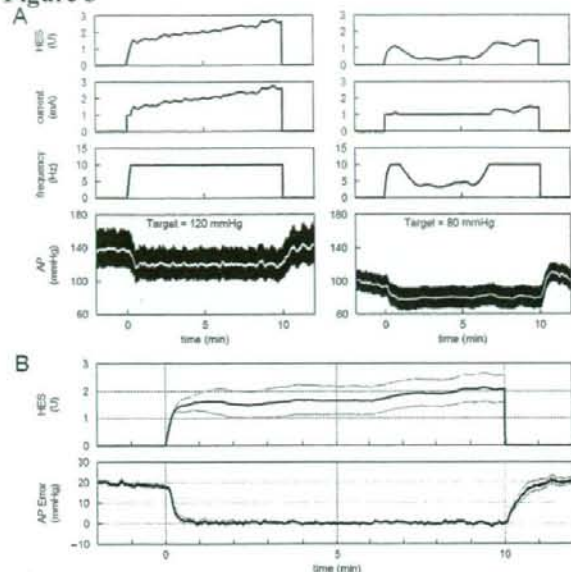
A: Results of 10-min feedback control of arterial pressure (AP) by hind-limb electrical stimulation (HES) obtained from 2 cats. In each cat, the target AP was set at 20 mmHg below the baseline AP value. The current and frequency of HES were automatically adjusted to keep the AP at the target level. **B:** HES command and the error signal between the target AP and measured AP averaged from 8 cats. The thick and thin lines indicate mean±SE values, respectively.

Figure 6
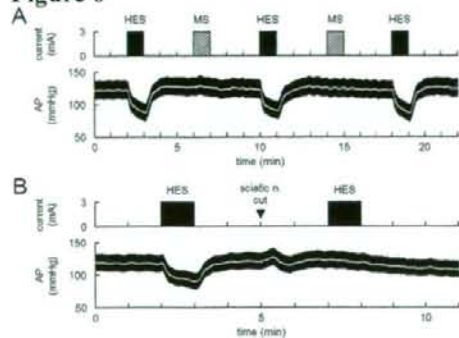
A: Effects of electrical stimulation of the triceps surae muscle (MS) in comparison to hind-limb electrical stimulation (HES). Although muscle twitching was observed, there was no change in arterial pressure (AP) during MS. **B:** Effects of sectioning the ipsilateral sciatic nerve on the HES-induced changes in AP. After the severance of the ipsilateral sciatic nerve, HES no longer produced significant hypotension.

Figure 7
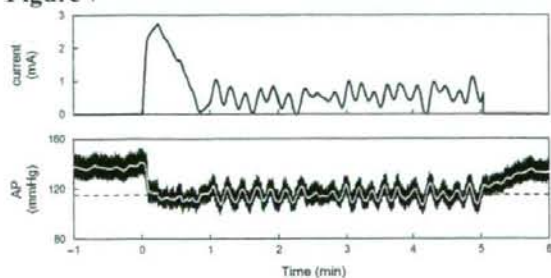
Typical recordings showing failure of controlling the intensity of the hind-limb electrical stimulation during the course of controller development. In this experimental run, only the stimulus current was controlled with a fixed stimulus frequency at 10 Hz. The controller showed on-off type controller behavior once the arterial pressure (AP) approached the target level. The horizontal dashed line indicates the target AP level.

Mini Review
Artificial Neural Interfaces for Bionic Cardiovascular Treatments

Authors: Toru Kawada, MD, PhD, and Masaru Sugimachi, MD, PhD.

Affiliations: Department of Cardiovascular Dynamics, Advanced Medical
                Engineering Center, National Cardiovascular Center Research
                Institute, Osaka 565-8565, Japan

Running head: Artificial Neural Interfaces

Correspondence:
                Toru Kawada, MD, PhD.
                Department of Cardiovascular Dynamics, Advanced Medical
                Engineering Center, National Cardiovascular Center Research
                Institute, Osaka 565-8565, Japan
                phone: +81-6-6833-5012
                Fax: +81-6-6835-5403
                e-mail: torukawa@res.ncvc.go.jp

Abstract

An artificial nerve, in the broad sense, may be conceptualized as a physical and logical interface system that reestablishes the information traffic between the central nervous system and peripheral organs. Studies on artificial nerves targeting the autonomic nervous system are in progress to explore new treatment strategies for several cardiovascular diseases. First, we identified the rule for decoding native sympathetic nerve activity into heart rate using a transfer function analysis, and established a framework for a neurally regulated cardiac pacemaker. Second, we designed a bionic baroreflex system to restore the baroreflex buffering function using electrical stimulation of the celiac ganglion in a rat model of orthostatic hypotension. Third, based on the hypothesis that autonomic imbalance aggravates chronic heart failure, we implanted a neural interface into the right vagal nerve and demonstrated that intermittent vagal stimulation significantly improved the survival rate in rats with chronic heart failure following myocardial infarction. Although several practical problems need to be resolved, such as those relating to the development of electrodes feasible for long-term nerve activity recording, studies on the artificial neural interfaces with the autonomic nervous system have great possibilities in the field of cardiovascular treatment. We expect further development of the artificial neural interfaces as novel strategies to cope with cardiovascular diseases resistant to conventional therapeutics.

Key words: autonomic nervous system, arterial pressure, orthostatic hypotension, heart failure, transfer function

Introduction

Peripheral nerves are the pathways that convey information from peripheral organs to the central nervous system and commands from the central nervous system to peripheral organs. Damages to the peripheral nerves caused by injuries or diseases are disadvantageous to the living organs. In the narrow sense, an artificial nerve would indicate a replacement of the nerve fiber or nerve bundle with artificial materials capable of conducting nerve impulses. In the broad sense, the artificial nerve may be conceptualized as a physical and logical interface system that reestablishes the information traffic between the central nervous system and peripheral organs. Studies on artificial eyes and ears aim to restore sensory functions by building neural interfaces between artificial sensory devices and sensory nerves, the brainstem or the sensory cortex.[1-4] Studies on functional electrical stimulation aim to restore motor functions via electrical activation of lower motor neurons through stimulation of axons in peripheral nerves or within the spinal cord.[5] Functional electrical stimulation may also be applied directly to skeletal muscles.[6] In addition to these studies on artificial nerves relating to the sensory and motor systems, studies targeting the autonomic nervous system are in progress to explore new treatment strategies for cardiovascular diseases.

The heart has automaticity, which allows it to continue beating even in the absence of regulation by the autonomic nervous system. Loss of autonomic nervous regulation does not instantly terminate the circulation. In this sense, the significance of studies on the artificial nerves targeting the autonomic nervous system to treat cardiovascular diseases may be somewhat elusive compared with the studies related to the sensory and motor systems. However, the disruption of the autonomic nervous regulation critically affects activities of daily living. As an example, patients with severe orthostatic hypotension cannot maintain arterial pressure to keep consciousness during sitting or standing position and are forced to become bedridden. An artificial neural interface with the autonomic nervous system is expected to be an effective countermeasure to such diseased conditions. In this article, we will review our researches targeting the autonomic nervous system to treat cardiovascular diseases.

Neurally regulated cardiac pacemaker

A regulatory system of living organs, such as the autonomic nervous system, senses multiple physiological variables and controls the effector organs

accordingly. The first requirement in the development of an artificial neural interface system that can control effector organs is to decode native neural impulses quantitatively and interpret the commands from the central nervous system to the effector organs. In reference to the sympathetic heart rate control, although sympathetic activation is known to increase heart rate, a qualitative understanding of the input-output relationship is of little use in the development of a neurally regulated cardiac pacemaker. To examine the input-output relationship between these two variables, we measured left cardiac sympathetic nerve activity and heart rate in anesthetized rabbits.[7] The cervical vagal nerves were sectioned to avoid any vagal effects on heart rate. By imposing random pressure variations on the isolated carotid sinuses, we perturbed sympathetic nerve activity via the carotid sinus baroreflex. Plotting the instantaneous heart rate versus sympathetic nerve activity did not reveal any apparent correlations between the two signals (Fig. 1A). This is because the current heart rate is not determined solely by current sympathetic nerve activity but also influenced by the past history of sympathetic nerve activity.

In order to identify the dynamic input-output relationship between sympathetic nerve activity and heart rate, including the effect of past history, we employed a white noise analysis used in the engineering field (see Appendix for details). The transfer function from sympathetic nerve activity to heart rate approximated a low-pass filter (Fig. 1B). The response of heart rate became smaller and more delayed as the frequency of input perturbation increased. Berger *et al.* identified similar low-pass filter-like characteristics of sympathetic heart rate control using random electrical stimulation of the cardiac sympathetic nerve in anesthetized dogs.[8] When we calculated the impulse response via the inverse Fourier transform of the transfer function (see Appendix for details), the impulse response revealed a significant positive value for approximately 10 s. This result indicates that sympathetic nerve activity at any given time influences heart rate for approximately 10 s in rabbits (Fig. 1B). Once the impulse response is obtained, we can predict the output signal (heart rate) from the convolution integral between the input signal (sympathetic nerve activity) and the impulse response. Heart rate predicted from the measured sympathetic nerve activity demonstrated good agreement with the measured heart rate (Fig. 1C). Although several practical problems need to be resolved, accurate prediction of the instantaneous heart rate makes the framework using the transfer function extremely attractive as a principle for designing a neurally regulated cardiac

pacemaker.

Further comments on the transfer function analysis would help in-depth understanding. In the above-mentioned study,[7] we calculated the transfer function from left cardiac sympathetic nerve activity to heart rate. In reality, a branch of the left cardiac sympathetic nerve was sectioned and the nerve activity was recorded from the proximal end of the sectioned nerve. Therefore, the sympathetic nerve from which activity was recorded could not affect heart rate at the time of experiment. In addition, because the sinus node is predominantly innervated by the right cardiac sympathetic nerve, changes in heart rate are produced mainly by the right cardiac sympathetic nerve.[9] An implicit assumption of the study was that left cardiac sympathetic nerve activity could be the proxy of total sympathetic nerve activity that regulated heart rate. High coherence between left cardiac sympathetic nerve activity and heart rate is in support of this assumption (Fig. 1B). If the heart rate was regulated by a mechanism totally independent of left cardiac sympathetic nerve activity, the coherence function must have shown values close to zero. We verified our assumption by simultaneously recording left and right cardiac sympathetic nerve activities.[10] There was no apparent laterality of cardiac sympathetic nerve activities in response to dynamic carotid sinus baroreflex perturbation. The laterality observed in the sympathetic effects on the heart rate and ventricular contractility[9] may be mainly attributable to the different distributions of left and right cardiac sympathetic nerves within the heart.

Bionic baroreflex system

Multiple system atrophy (Shy-Drager syndrome) is caused by a disorder of the autonomic nervous system. Shy-Drager patients suffer from severe orthostatic hypotension because of the lack of a baroreflex buffering effect. Although counter measures to orthostatic hypotension are used such as administration of pressor agents and volume expansion, these treatments may induce supine hypertension. Ideal treatment would increase arterial pressure only when necessary, i.e., a position-dependent or more accurately a pressure-dependent pressor effect is required. In Shy-Drager patients, plasma noradrenaline levels are nearly normal in supine position and increase following tyramine administration, indicating that peripheral postganglionic sympathetic nerves are relatively spared but only weakly activated by postural changes.[11] If we can encode the information necessary for arterial pressure regulation and

deliver those signals to the postganglionic sympathetic system, orthostatic hypotension may be prevented using artificial sympathetic neural interventions.

Because a single nerve fiber discharges according to an all-or-nothing principle, it conveys information by frequency modulation. In contrast, multiple-fiber recording of a nerve bundle exhibits both frequency and amplitude modulations. This is because the amplitude of multiple-fiber recording is the weighted sum of concurrently discharging nerve impulses in the nerve bundle. Nerve fibers adjacent to the electrodes will contribute more to the amplitude generation. The ultimate goal of an artificial neural interface would be to create a respective interface with each nerve fiber in the bundle that could reproduce both the frequency and amplitude modulations. It is unrealistic at present, however, to establish such a complete interface, given the large number of nerve fibers and the small size of the interface.

An alternative strategy for neural interventions is to create a single neural interface to the whole nerve bundle and treat the system from nerve bundle stimulation to the effector response as a peripheral effector system. Using the electrical stimulation of the celiac ganglion, we explored the development of an artificial vasomotor center to restore normal arterial baroreflex function in rats with central baroreflex failure.[12,13] We first identified the dynamic characteristics of the carotid sinus baroreflex by imposing random pressure perturbations on the isolated carotid sinuses. The transfer function from baroreceptor pressure input to arterial pressure is defined as the native baroreflex function $[H_{Native}(f)]$. Next, we imposed random electrical stimulations on the celiac ganglion and quantified the transfer function from electrical stimulation to the arterial pressure response $[H_{Stim \to AP}(f)]$. Because the celiac ganglion governs a large abdominal vascular bed, electrical stimulation of the celiac ganglion effectively increased arterial pressure. The transfer function of the controller $[H_{Bionic}(f)]$ was then determined in the frequency domain to fulfill the following equation (Fig. 2A, see Appendix for details).

$$H_{Bionic}(f)H_{Stim \to AP}(f) = H_{Native}(f)$$

In a typical experimental result (Fig. 2B), a head-up tilt did not decrease arterial pressure substantially in the rat with normal baroreflex. In contrast, the same head-up tilt caused significant hypotension in the rat with baroreflex failure. Activation of the bionic baroreflex system was able to restore the baroreflex buffering to a degree similar to that observed in the rat with normal baroreflex.

Note that native neural discharge of the celiac ganglion was not

recorded to develop the bionic baroreflex system,[12,13] whereas recording of the native cardiac sympathetic nerve activity was essential for the development of a neurally regulated cardiac pacemaker.[7] This distinction comes from the fact that the artificial vasomotor center was designed to control the peripheral effector system via electrical stimulation of the celiac ganglion to exert an arterial pressure response. A variety of interventions capable of changing arterial pressure can be treated as a peripheral effector of the bionic baroreflex system. We identified the transfer function from epidural spinal cord stimulation to the arterial pressure response and demonstrated that the bionic baroreflex system using epidural spinal cord stimulation could prevent orthostatic hypotension in anesthetized cats.[14] Yamasaki et al. applied the bionic baroreflex system using epidural spinal cord stimulation to prevent hypotension after sudden deflation of the thigh tourniquet in knee joint surgery.[15] Gotoh et al. demonstrated that an artificial neural interface with the vasomotor center (rostral ventrolateral medulla) provided rapid and precise control of arterial pressure in conscious rats.[16]

Bionic treatment against chronic heart failure

The autonomic nervous system plays an important role in maintaining the circulation under normal physiological conditions. Sympathetic activation and vagal withdrawal during exercise are beneficial to increase cardiac output in response to increased oxygen demand. Native autonomic regulation, however, does not always operate properly under diseased conditions. Heart failure develops when the heart can no longer provide adequate cardiac output to meet the oxygen demand. While sympathetic activation and vagal withdrawal help compensate for the reduced cardiac performance initially, sympathetic overactivity and vagal withdrawal eventually exacerbate the failing heart, resulting in sympathovagal imbalance and the vicious circle of chronic heart failure. Based on the pathological observation that sympathetic overactivity worsens heart failure, beta-adrenergic blockers and angiotensin converting enzyme inhibitors have been used as treatment. Although beta-blockers were long considered to be contra-indicated in heart failure, these drugs were ultimately demonstrated to improve outcome and are now established treatments.[17] Nevertheless, the therapeutic effect of sympathetic blockade is not always sufficient.

We hypothesized that vagal activation would also help terminate the vicious circle in chronic heart failure, and examined if vagal nerve stimulation

could treat chronic heart failure.[18] In halothane-anesthetized rats, the left coronary artery was ligated to produce myocardial infarction. One week later, a telemetry system to record arterial pressure and heart rate and a tele-stimulator system to stimulate the right vagal nerve were implanted under anesthetized conditions. Another week later (at 14 days after myocardial infarction), surviving rats were divided into vagal stimulation and control groups. In the vagal stimulation group, the right cervical vagal nerve was stimulated intermittently (10-s stimulation per minute) for 6 weeks. The intensity of vagal stimulation was adjusted to decrease heart rate by 20-30 beats/min. A 140-day follow-up revealed that vagal stimulation significantly increased the survival rate (Fig. 3). Although we did not directly treat the failing heart, the artificial neural interface to the vagal nerve ameliorated heart failure, thereby improved the survival rate.

The mechanisms by which vagal stimulation ameliorates chronic heart failure are not fully understood. Because vagal stimulation decreases heart rate, myocardial oxygen consumption is reduced. Vagal stimulation can also reduce ventricular contractility via the antagonism to the sympathetic effect,[19] which may also help reduce myocardial oxygen demand. Vagal stimulation shows anti-fibrillatory effect during ischemic insult in healed myocardial infarction in conscious dogs.[20] In acute myocardial ischemia, vagal stimulation reduces the accumulation of noradrenaline in the myocardial interstitium of the ischemic region.[21] Because catecholamines have cardiotoxicity,[22] reducing myocardial interstitial noradrenaline levels in the ischemic region may be cardioprotective. Vagal stimulation also reduces the protein levels of endogenous active matrix metalloproteinase-9 during ischemia-reperfusion injury,[23] which may contribute to the inhibition of ventricular remodeling. Because acetylcholine concentrations in the ischemic myocardium are increased via a local releasing mechanism that is independent of voltage dependent calcium channels,[24,25] vagal stimulation can only induce small additional increases in acetylcholine concentrations in the ischemic region.[21] Given the profound ameliorative effect of vagal stimulation in chronic heart failure,[18] the target of vagal effect may be the ischemic border zone, rather than the ischemic zone itself. Also, the vagal afferent pathway may modify the central nervous system to exert beneficial effects in chronic heart failure. Development of a new experimental method, such as that using reversible vagal blockade in conscious rats,[26] would help separate the afferent and efferent effects of vagal stimulation. Further studies are required to identify the mechanisms of cardioprotection by vagal stimulation.

Conclusion

In this review, we briefly summarized the studies of artificial neural interfaces targeting the autonomic nervous system with the goal of treating several cardiovascular diseases. In all of the studies discussed, creating a logical and physical interface with the autonomic nervous system is the key to effective cardiovascular treatment. In relation to the logical interface, we have demonstrated that the application of the white noise analysis was useful to decode and encode information for the autonomic nervous system. In relation to the physical interface, electrodes truly capable of long-term recording have not yet been realized. Although we examined the application of sieve-type nerve regeneration electrodes for stimulating and recording the autonomic nerves, further refinements are necessary for practical use. Studies of artificial neural interfaces with the autonomic nervous system are intriguing and have immense possibilities in the field of cardiovascular treatment. We expect further development of artificial neural interfaces as novel strategies to manage cardiovascular diseases that are resistant to conventional therapeutics.

Appendix A. Transfer function analysis

We resampled input-output data of sympathetic nerve activity and heart rate at 10 Hz, and segmented them into 8 sets of 50%-overlapping bins of 1024 points each. For each segment, a linear trend was subtracted and a Hanning window was applied. A fast Fourier transform was performed to obtain the frequency spectra of the input and output. Ensemble averages of input power spectra [$S_{XX}(f)$], output power spectra [$S_{YY}(f)$], and the cross spectra between the input and output [$S_{YX}(f)$] were then calculated. The transfer function was estimated from the following equation.[27]

$$H(f) = \frac{S_{YX}(f)}{S_{XX}(f)} \tag{A1}$$

The coherence function between the input and output was calculated from the following equation.[27]

$$Coh(f) = \frac{|S_{YX}(f)|^2}{S_{XX}(f)S_{YY}(f)} \tag{A2}$$

The coherence function ranges from zero to unity. Zero coherence indicates total independence between the input and output. Unity coherence indicates a perfect linear dependence of the output on the input.

Once the transfer function was identified, we could calculate the impulse response of the system $[h(\tau)]$ via inverse Fourier transform of the transfer function. We then predicted the system response $[y(t)]$ to an input signal $[x(t)]$ from the convolution integral between $h(\tau)$ and $x(t)$ according to the following equation.

$$y(t) = \int_0^t h(\tau)x(t-\tau)d\tau \qquad (A3)$$

Although the above convolution integral predicts changes in the output signal in response to changes in the input signal, it cannot usually predict the direct current component or mean value of the output signal. In the case of the sympathetic heart rate control, heart rate does not become zero in the absence of sympathetic stimulation. In the prediction (Fig. 1C), we added the mean value of the measured heart rate to the output signal of the convolution integral to predict the absolute heart rate value.

Appendix B. Designing a bionic baroreflex system

The transfer function of the native baroreflex $[H_{Native}(f)]$ determined the dynamic input-output relationship between baroreceptor pressure input $[P_{Input}(f)]$ and arterial pressure $[AP(f)]$ in the frequency domain.

$$AP(f) = H_{Native}(f)P_{Input}(f) \qquad (B1)$$

The transfer function from the stimulus command to arterial pressure $[H_{Stim \to AP}(f)]$ determined the dynamic input-output relationship between the stimulus command $[C_{Stim}(f)]$ and arterial pressure in the frequency domain.

$$AP(f) = H_{Stim \to AP}(f)C_{Stim}(f) \qquad (B2)$$

The transfer function of the bionic baroreflex $[H_{Bionic}(f)]$ determined the dynamic input-output relationship between baroreceptor pressure input and stimulus command in the frequency domain.

$$C_{Stim}(f) = H_{Bionic}(f)P_{Input}(f) \qquad (B3)$$

From equations B2 and B3, the arterial pressure regulation by the bionic baroreflex can be described as follows.

$$AP(f) = H_{Stim \to AP}(f)H_{Bionic}(f)P_{Input}(f) \qquad (B4)$$

Comparison of equations B1 and B4 determined that the bionic baroreflex should fulfill the following equation to reproduce the native baroreflex function.